Princeton Plasma Physics Laboratory

PPPL- 4580

PPPL- 4580

# Magnetic Diagnostics for Equilibrium Reconstructions in the Presence of Nonaxisymmetric Eddy Current Distributions in Tokamaks

L. Berzak, A. D. Jones, R. Kaita, T. Kozub, N. Logan, R. Majeski,
J. Menard, and L. Zakharov

December, 2010

Prepared for the U.S. Department of Energy under Contract DE-AC02-09CH11466.

# Princeton Plasma Physics Laboratory
# Report Disclaimers

---

## Full Legal Disclaimer



## Trademark Disclaimer



---

# PPPL Report Availability

## Princeton Plasma Physics Laboratory:

http://www.pppl.gov/techreports.cfm

## Office of Scientific and Technical Information (OSTI):

http://www.osti.gov/bridge

---

**Related Links:**

**U.S. Department of Energy**

**Office of Scientific and Technical Information**

**Fusion Links**

# Magnetic diagnostics for equilibrium reconstructions in the presence of nonaxisymmetric eddy current distributions in tokamaks (invited)[a)]

L. Berzak,[b)] A. D. Jones, R. Kaita, T. Kozub, N. Logan, R. Majeski, J. Menard, and L. Zakharov
*Princeton Plasma Physics Laboratory, P.O. Box 451, Princeton, New Jersey 08543, USA*

(Presented 19 May 2010; received 14 May 2010; accepted 26 July 2010; published online 14 October 2010)

The lithium tokamak experiment (LTX) is a modest-sized spherical tokamak ($R_0$=0.4 m and a =0.26 m) designed to investigate the low-recycling lithium wall operating regime for magnetically confined plasmas. LTX will reach this regime through a lithium-coated shell internal to the vacuum vessel, conformal to the plasma last-closed-flux surface, and heated to 300–400 °C. This structure is highly conductive and not axisymmetric. The three-dimensional nature of the shell causes the eddy currents and magnetic fields to be three-dimensional as well. In order to analyze the plasma equilibrium in the presence of three-dimensional eddy currents, an extensive array of unique magnetic diagnostics has been implemented. Sensors are designed to survive high temperatures and incidental contact with lithium and provide data on toroidal asymmetries as well as full coverage of the poloidal cross-section. The magnetic array has been utilized to determine the effects of nonaxisymmetric eddy currents and to model the start-up phase of LTX. Measurements from the magnetic array, coupled with two-dimensional field component modeling, have allowed a suitable field null and initial plasma current to be produced. For full magnetic reconstructions, a three-dimensional electromagnetic model of the vacuum vessel and shell is under development.  [doi:10.1063/1.3484488]

## I. INTRODUCTION

To achieve a viable fusion power plant, the engineering and physics challenges associated with the first wall must be mitigated and resolved. The limited viability of traditional materials has led to the investigation of novel first walls,[1,2] including liquid lithium plasma-facing components (PFCs).[3]

The first experiments utilizing lithium began with straightforward wall-conditioning techniques.[4–6] These experiments motivated more extensive lithium research programs such as liquid lithium rail limiters.[7,8] The current-drive experiment-upgrade (CDX-U) at the Princeton Plasma Physics Laboratory (PPPL) investigated the effects of a heated, toroidal tray limiter filled with 2000 $cm^2$ of liquid lithium.[9] CDX-U noted increased fueling requirements to maintain plasma density, decreased loop voltage requirements, and a factor of 6 improvement in energy confinement time subsequent to the introduction of liquid lithium.[10] Promising results from CDX-U have motivated fully liquid lithium PFCs in the lithium tokamak experiment (LTX) at PPPL.

## II. OVERVIEW OF THE LITHIUM TOKAMAK EXPERIMENT

Building upon the results of CDX-U, LTX is a modest-sized ($R_0$=0.4 m, a=0.26 m, $\kappa \approx 1.6$, and $B_T \approx 2$ kG) spherical tokamak (ST) designed to investigate the low-recycling operating regime reached via liquid lithium PFCs. In order to have a nearly full liquid lithium wall, LTX has a close-fitting, conformal shell inside a cylindrical vacuum vessel (Fig. 1). The shell is constructed in four electrically isolated segments (two upper halves and two lower halves) from 3/8 in. thick copper, plasma-sprayed with nickel, and explosively bonded to 3/16 in. thick stainless steel. The stainless steel faces the plasma and will be evaporatively coated with lithium. Heaters on the non-plasma-facing, nickel-sprayed copper side of the shell maintain the shell temperature above the melting point of lithium. Because copper has a high thermal conductivity, the primarily copper shell will provide a hot, uniform temperature first wall. When the shell is coated, it will provide a liquid lithium area of 5 $m^2$, more than 85% of the plasma last-closed-flux surface.

Although the shell will allow LTX to access a new, low-recycling operating regime, the shell's presence introduces many challenges to plasma operations. Diagnostic access to the plasma is limited by the close-fitting shell, and the available volume for plasma movement is reduced emphasizing the importance of plasma control and stability. Moreover, even though the shell has two 22.5° toroidal breaks and both inboard and outboard poloidal breaks, the high electrical conductivity of the copper permits significant, nonaxisymmetric eddy currents to flow. These eddy currents delay field penetration into the plasma volume and produce field that affects both magnetic diagnostics' signals and the plasma itself. Eddy currents strongly influence the low current plasma start-up phase.

[a)] Invited paper, published as part of the Proceedings of the 18th Topical Conference on High-Temperature Plasma Diagnostics, Wildwood, New Jersey, May 2010.

[b)] Electronic mail: lberzak@pppl.gov.

 

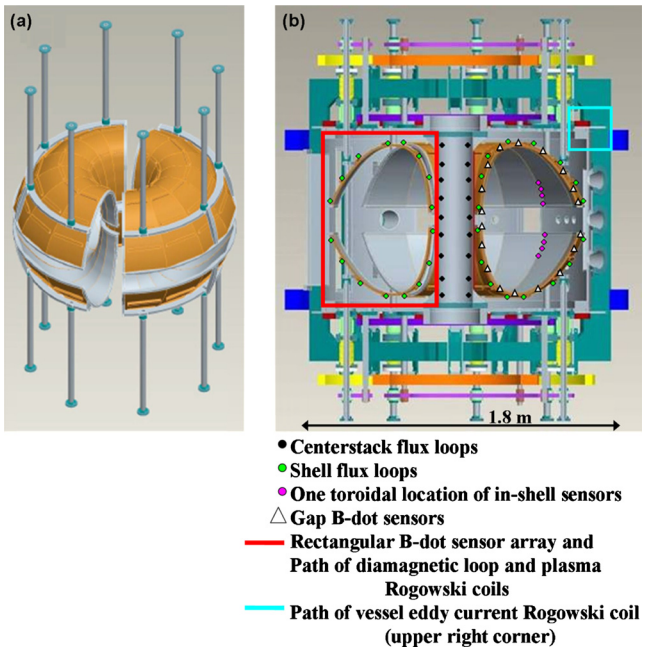


FIG. 1. (Color online) (a) LTX shell quadrants with support legs. Two toroidal breaks as well as inboard and outboard poloidal breaks can be seen. (b) Schematic of LTX showing field coils, vacuum vessel, shell, and approximate placement of magnetic diagnostics as indicated in legend.

For prelithium operations, LTX has utilized short-pulse (14 ms peak-to-peak) capacitor banks to power the Ohmic system. These banks provide loop voltage limited to less than 6 V, and the Ohmic waveform is strictly determined by the capacitor banks' *LRC* circuit. Eddy currents are exacerbated by the 4.5 MA/s ramp rate of the Ohmic current. A new, programmable insulated gate bipolar transistor H-bridge power supply-controlled capacitor bank is under construction, and will provide higher power for increased loop voltage and allows the Ohmic pulse waveform, including ramp rate, to be controlled. However, with either power supply, eddy currents will be three-dimensional in nature and must be taken into account during magnetic calibration, equilibrium code validation, and plasma operations.

The data analysis of magnetic diagnostics' signals, in conjunction with the development of two-dimensional modeling, has yielded an understanding of the conducting, double-walled vessel and shell system of LTX. As a result, plasmas of 15 kA, 5 ms have been achieved with the short-pulse Ohmic capacitor banks and no wall-conditioning. After this start-up phase of LTX, the programmable power supply will be installed. With the new power supply and the introduction of lithium, discharges of 150 kA, 25 ms are expected.

## III. MAGNETIC DIAGNOSTICS

The complicated LTX double-walled system requires a high density of magnetic diagnostics in order to elucidate and quantify the resulting complicated field patterns and to develop a plasma start-up scenario in the presence of these nonaxisymmetric currents. For the purpose of quantifying eddy currents and calculating highly constrained equilibrium reconstructions, LTX has an extensive set of magnetic diagnostics, including 27 flux loops, 4 saddle loops, 102 B-dot coils, 2 plasma Rogowski coils, a vessel current Rogowski coil, and a diamagnetic loop. The magnetic diagnostics are designed to withstand incidental contact with liquid lithium as well as to survive shell operation up to 500 °C. Sensors and their protective housing are therefore fabricated from robust materials with heat and lithium resistance, including stainless steel and yttria-stabilized magnesium oxide. The magnetic sensors have been tested during shell heating and during calibration shots, and they have performed as designed.

The magnetic diagnostic system provides full coverage of the poloidal cross-section as well as data at several toroidal angles, revealing toroidal asymmetries during plasma operation. All sensor locations are mirror-imaged on the top and bottom shells. This design has been valuable in elucidating up-down asymmetries in machine construction and during discharge development. The various locations of the diagnostics were chosen so as to minimize the distance between the diagnostic and the plasma. The design of the magnetic array maintains the electrical isolation between the four shell quadrants and between the shells and the vacuum vessel.

The initial design of the magnetic diagnostics has previously been briefly described.[11] The following sections provide details of the final diagnostic design and operation.

### A. Flux loops

There are 27 flux loops installed in LTX. These flux loops are used to validate the model of LTX in the equilibrium codes, design poloidal fields for plasma start-up, and constrain plasma reconstructions. The set of flux loops includes 11 flux loops spaced evenly in the air-side of the centerstack. An unintegrated centerstack flux loop located at the horizontal midplane measures the loop voltage available to drive plasma current.

A separate series of flux loops (eight mounted to the upper shell halves and eight mounted to the lower shell halves) is mounted directly to the non-plasma-facing side of the shell. The locations of these shell flux loops are thus only ~3/8 in. from the plasma. The shell flux loops provide full coverage (inboard to outboard) of the plasma poloidal cross-section. The data collected from the shell flux loops is used to diagnose the vertical field null during plasma start-up and to constrain plasma reconstructions.

LTX also has a set of saddle loops. There are four of these rectangular flux loops spanning a toroidal shell gap (two mounted to the upper shell toroidal gap edges and two mirrored on the lower gap). These loops are mounted such that the measured flux is the flux through the toroidal gap. Because of their location across a toroidal gap, the design for the saddle loops provides physical support as the diagnostic crosses the gap, protection from lithium contact, and electrical isolation. Similar to the design for the shell flux loops,[11] the saddle loops are housed in stainless steel tubing, segmented to prevent driving currents and covered by tubes of magnesium oxide. These loops have two turns with a center-tap tied to electronics ground, a design that improves differential signal balance, prevents capacitive coupling, and pro-

vides noise immunity by reducing dependence on the common mode rejection of the amplifier circuit. The saddle loop signals are used to diagnose eddy currents in the shells by providing a direct measurement of flux into the toroidal gap.

### B. B-dot coils

The LTX B-dot array includes a total of 102 sensors. This sensor array is comprised of single and double-axis probes, and provides full coverage of the plasma cross-section. The sensors provide data from various toroidal angles and are located internal and external to the shell and in-shell gaps.

One set of sensors in the B-dot array is the in-shell coil set. There are 30 in-shell coils divided into sets of ten, located at three distinct toroidal angles. The toroidal angles (79°, 259°, and 281°) were selected to provide the capability to remove $m=2$ magnetohydrodynamic mode contributions from signals as well as to compare measurements of poloidal field at "neighboring" shell segments.

Each set of ten is comprised of two sets of five sensors each, with five sensors on the upper shell measuring outboard poloidal field and five sensors correspondingly on the lower shell. These sensors are small in size (length of ~2.5 cm and diameter of ~4 mm) and are housed in a length of thin-walled stainless steel tubing welded to the plasma-facing side of the shell. The tube has a wall thickness of 0.01 in. yielding an $L/R$ time on the order of 1 $\mu$s, preventing the tube from influencing the measured signals. The tubing lies just outside the plasma last-closed-flux surface and inside the shell, placing the sensors within millimeters of the plasma. The in-shell sensor array provides a dense measurement of outboard poloidal field at several toroidal locations, with minimal shell influence due to proximity to the plasma.

The ex-shell coil set is a corresponding array of sensors. The ex-shell sensor array is composed of a total of 12 sensors divided into two toroidal sets, with 3 sensors on the upper shell and 3 sensors on the lower shell at each toroidal location. This set is comprised of sensors of the same size and fabrication as the in-shell sensors, but ex-shell sensors are mounted to the non-plasma-facing side of the shell. The ex-shell coils' toroidal locations match two of the in-shell sensor locations and mimic the poloidal position of six in-shell coils at these toroidal locations. The ex-shell coils provide a dense measurement of outboard poloidal field and, through a comparison to the in-shell coils, a direct measurement of surface current flowing on the shell.

To provide a measurement of magnetic field with minimal shell influence while covering the full poloidal cross-section, an array of 18 two-axis probes is mounted in one of the toroidal shell gaps. These gap sensors are located in the center of the toroidal gap, and are protected from lithium by stainless steel covers and the plasma-sprayed tungsten tabs on which they are mounted. Nine probes are mounted in the upper shell toroidal gap, with nine probes at locations which mirror them in the lower shell gap. These probes measure both poloidal and radial fields, and as such can be used to decompose the measured fields into a vertical component. This decomposition provides a measure of the vertical field across the full poloidal cross-section. The radial field sensors also measure the bulge of magnetic field into the toroidal gap.

There is also a rectangular array of 26 sensors mounted in vacuum outside a toroidal shell gap. This array is comprised of a vertical array of sensors along the centerstack, two radial arrays lying against the top and bottom vessel flanges, and a vertical outboard array along the vacuum vessel wall. These sensor sets are all re-entrant to allow air-cooling if necessary. The data collected from these sensors are valuable for validating the location and size of the inboard poloidal field coils relative to the shell in the model, a prerequisite for accurate equilibrium reconstructions.

### C. Additional magnetics

LTX has two plasma current Rogowski coils, fabricated from high-temperature materials (specified to 250 °C or above) including a 2.87 mm Teflon former, glass fiber outer sleeving, and 301 °C solder, and is housed in re-entrant tubing to allow air-cooling. These Rogowski coils are inside the vacuum vessel and surround the shells without contacting them. The two coils are located at distinct toroidal locations, such that one surrounds the center of the shells while the second lies next to the shell edges at a toroidal gap. This design provides the opportunity to elucidate asymmetries in toroidal plasma current due to the shell.

In addition, there is a vessel eddy current Rogowski coil. This coil is re-entrant and surrounds an upper vacuum vessel corner. The "corner" Rogowski provides a direct measurement of vessel eddy currents. Because the vacuum vessel itself is highly nonaxisymmetric, the corner Rogowski coil measurement is not fully representative of the current distribution across the entire vessel; the measurement does, though, provide a measure of the magnitude and timing of the induced eddy currents.

LTX also has a diamagnetic loop inside the vacuum vessel outside the shells in order to measure $\beta$ and plasma stored energy. The diamagnetic loop is oriented radially as defined by the centers of circular ports on the top and bottom flanges. Mounted utilizing these machine reference points, the internal diamagnetic loop is aligned to an accuracy of approximately 1 mm. There is also an associated compensation coil outside the vacuum vessel to assist with removing toroidal field coil contribution from the diamagnetic loop measurement. This compensation coil is oriented radially by mounting in the center of a rectangular flange and is aligned to external machine reference points with submillimeter accuracy. The rectangular flange is located below a toroidal gap in the shell at a position of symmetry on the vacuum vessel to minimize eddy current contributions to the signal.

## IV. TWO-DIMENSIONAL MODELING OF LTX

Because of the complexity and computational expense of full three-dimensional simulations, a two-dimensional electromagnetic model for the LTX double-walled conducting structure has been developed. Simulations using this two-dimensional model will, by necessity, miss three-dimensional

effects such as field in the toroidal shell gaps. However, this model has been proven valuable for LTX start-up design and initial discharge development, and has been validated against measured magnetic diagnostics' signals. This new model successfully reduces the three-dimensionality of LTX, such that an inherently two-dimensional code algorithm can be used to simulate LTX discharges and calculate initial plasma reconstructions.

The utilized code algorithm, LRDFIT (Inductance (L)-resistance (R) circuit model with data fitting capabilities), is used to model National Spherical Torus Experiment (NSTX) discharges,[12,13] and has now been developed for usage with LTX. LRDFIT models the shell cross-section as an array of two-dimensional parallelograms, each with individually assigned inductance and resistance values. The parallelograms are divided into rectangular elements, and the field due to a nondelta function current distributed across a rectangular cross-section conductor is calculated. The nondelta function treatment of current in conductors permits the accurate calculation of field quantities inside the conductors themselves. The circuit equations are diagonalized to retain explicitly all $L/R$ time scales.

To reduce the three-dimensional nature of LTX to a two-dimensional approximation, the resistance of shell parallelograms is adjusted from an initial value calculated using the resistivity of oxygen-free high thermal conductivity copper. A coefficient with a major radius dependence is applied to the resistivity of each element. Although empirical, this coefficient allows the different path lengths for inboard and outboard localized currents coupled by the return path for current in the poloidal direction to be taken into account. The optimal distribution of resistivity coefficients from inboard to outboard has been determined using a weighted minimization of the difference between simulated and measured signals in regions of large field coil $dI/dt$. The resulting distribution accounts for the complicated path of currents flowing in the shell using a two-dimensional representation.

A comparison of simulated and measured sensor signals for a vacuum field-only pulse can be seen in Figs. 2(a)–2(c). Simulated signals are shown for LTX LRDFIT models without any shell structure, with a full resistivity shell structure, and with the resistivity adjusted shell structure. Error between simulated and measured signals is minimized by using the resistivity adjusted model [Fig. 2(c)].

Although inherently three-dimensional, currents in the shell can be simulated by LTX LRDFIT. In Fig. 2(d) caption, the "total" current value is a summation of current flowing in each shell element, a calculation of the net toroidal current flowing in the shell. Because of the toroidal gaps, a constraint is placed on the shell elements to force zero net current. This current must be zero in the machine, and as such, the resulting simulated value provides a measure of the error in the LTX LRDFIT model. Simulated toroidal current is indeed small, of order $10^{-13}$ kA. "Circulating" current is the sum of the absolute value of current flowing in each shell element, and provides the magnitude of the n=2 mode current flowing in each shell quadrant. By removing the n=1 shell current contribution, LTX LRDFIT is able to represent a three-dimensional, n=2, eddy current distribution in a reduced, two-dimensional form.

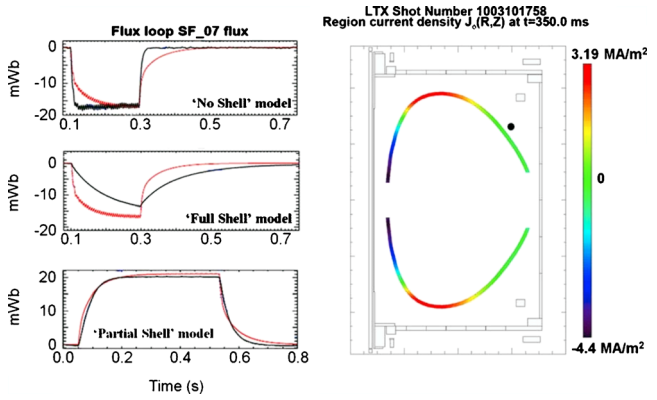


FIG. 2. (Color online) Measured [light gray (red)] and simulated (black) signals from an upper shell flux loop compared to various LTX LRDFIT models: (a) LTX LRDFIT model without a shell; (b) LTX LRDFIT model with full copper resistivity shell; (c) LTX LRDFIT "partial" shell model with adjusted resistivity values; (d) simulated shell current pattern; the location of compared shell flux loop in (a)–(c) is indicated by the black circle. At this time point (0.350 s) early in the Ohmic pulse, the simulated 'total' shell current is $4.45\times10^{-13}$ kA, while simulated circulating shell current is 16.6 kA.

Simulated, circulating shell currents can be compared to signals from the saddle loops and subtracted signals from the in- and ex-shell sensors (Fig. 3). Because LTX LRDFIT is a two-dimensional code, the fringe fields in the shell gap measured by the saddle loops cannot be directly simulated. However, the indirect comparison between measured saddle loop signal and simulated 'circulating' shell current demonstrates qualitative agreement. Conversion of the measured flux to current producing that flux based on the number of turns and

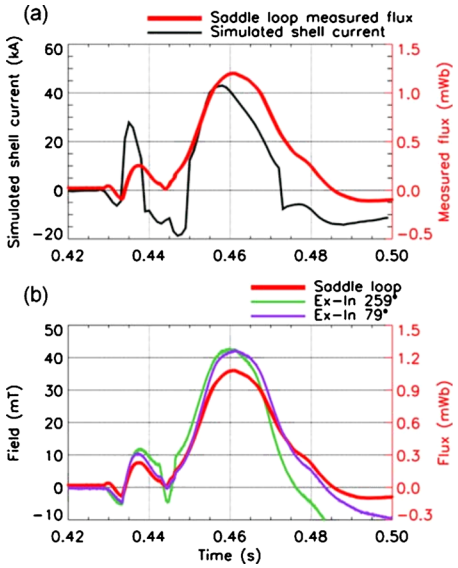


FIG. 3. (Color online) Plasma discharge extends from 0.443 to 0.448 s. (a) Comparison of simulated, "circulating" shell current and upper, inboard saddle loop measured flux. Note separate y-axes. (b) Comparison of measured saddle loop flux and subtracted ex- and in-shell sensor signals; sensors compared are mounted to upper shells. Note separate y-axes. Toroidal asymmetry in plasma field can be noted at 0.445 s between sensors located at toroidal angles of 79° and 259°.

cross-sectional area of the saddle loop provides good agreement with the magnitude of the simulated current. The measured saddle loop flux also temporally tracks the shell current with only a small phase lag.

The measured saddle loop flux coordinates well with the shell surface current measured by subtracting an in-shell sensor signal from a coordinating ex-shell sensor signal [Fig. 3(b)], yielding a measure of field due to current flowing between the two sensors. The magnitude of current flowing in the shell is not insignificant and with Ohmic-only pulses, it can reach as high as 40 kA. More typically, shell currents peak near 20 kA during a plasma discharge.

## V. DISCHARGE DEVELOPMENT

Because of the magnitude of the shell eddy currents, they cannot be neglected when designing plasma start-up and discharge development. Although not toroidally continuous, currents in the shells provide significant poloidal field, directed oppositely to field provided by the main poloidal field coils. This additional, oppositely directed field has both vertical and radial components and causes the plasma to be pulled apart and to be driven unstable. This effect is confirmed in visible fast camera images which show the plasma developing inboard limited, then moving outward and rapidly being pulled either up or down. Magnetic data also show clearly the plasma becoming localized to either the top or bottom shells, and initial plasma reconstructions (plasma toroidal current density singular value decomposition fit to data reconstruction) constrained by the in-shell sensors and shell flux loops show closed field lines high or low in the available plasma volume (Fig. 4).

With either the present, short-pulse Ohmic capacitor banks or the new, programmable power supply, the poloidal field must be carefully designed in order to balance the shell eddy currents and prevent destabilization of the plasma. Moreover, for an Ohmically driven ST such as LTX, start-up requires a field null near the peak in loop voltage to allow formation of the initial plasma current channel. It is therefore necessary to quantify the magnitude, vector direction, and timing of penetration of the vacuum magnetic fields and eddy currents generated inside the machine. The analysis of data from the magnetic array, coupled with two-dimensional modeling, yields a standardized approach to field null design and discharge development.

The analysis of data from the magnetic array begins with collecting a library of calibration shots, consisting of all poloidal field coils individually pulsed and pulsed in their operational pairs (e.g., main upper and lower vertical field coils are individually pulsed and then pulsed together). This library is composed of short pulse, capacitor bank-powered poloidal field coil shots and long-pulse (~400 ms) poloidal field coil shots, where possible. The former are collected for use in start-up scenario design. The latter allow sensor signals to reach an equilibrium state, which permits calculation of the eddy current decay times.

Signals from the long-pulse shots can be decomposed into separate field contributions. These distinct contributions include an initial square wave (the poloidal field coil contribution) and, although not qualitatively visible, three distinct exponential decays with associated time constants [Eq. (1)], calculated using the graphical peeling method and the method of moments.[14] Contributions to the sensor signal can be described by

$$B(t) = \alpha\Theta(t) + A_1 \exp^{-t/\tau_1} + A_2 \exp^{-t/\tau_2} + A_3 \exp^{-t/\tau_3}, \quad (1)$$

where $B(t)$ is the measured magnetic field, $\alpha\Theta(t)$ is the square wave contribution from the poloidal field coil itself, and $A_i$ and $\tau_i$ are the amplitude and time constants of each exponential contribution, respectively.

For LTX, the longest calculated time constant is 60 ms signifying that nearly 300 ms is required for these eddy currents to decay to 95% of their initial value. Because of this long time constant, it is important to take into account eddy current contributions to signals during magnetic diagnostic calibration. The longest time constant is followed by time constants of 30 ms (decay time of 150 ms) and 4 ms (decay time of 20 ms). These three distinct decay times can be related to circulating currents in the shell, skin time of the shell, and of vessel eddy current effects on the shell.

The library of calibration shots is subsequently expanded by a collection of poloidal field-only shots during shell heating tests (Fig. 5). The resistivity of copper increases by a factor of 2 as copper is heated from room temperature to 300 °C. Correspondingly, the decomposition of calibration shot signals indicates that the longest decay time, the decay time resulting from circulating shell currents, decreases by nearly a factor of 2 as the shell is heated to 300 °C. This

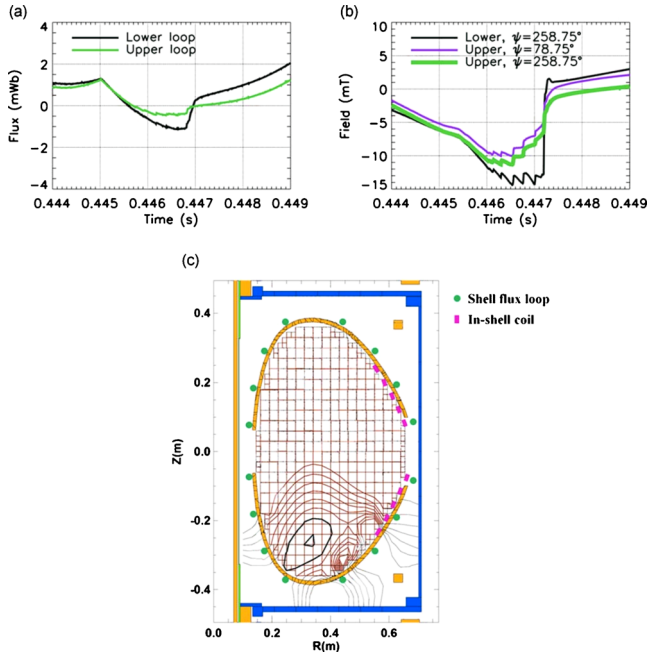


FIG. 4. (Color online) Discharge 1003261410 becomes localized to the bottom shells; the discharge extends from 0.442 to 0.447 s. (a) Comparison of upper and lower shell flux loops. (b) Comparison of upper and lower in-shell coils at different toroidal, $\psi$, locations. (c) Initial plasma reconstruction showing the combined contours of applied and plasma-generated poloidal field. At t=446.0 ms, the plasma current is near its peak value of 11 kA. Reconstructed field contours throughout the majority of the cross-section are open; closed contours, demonstrating where the plasma current is located, are highlighted in the lower shell. Approximate locations of diagnostics used to constrain the reconstructions are shown as indicated in the legend.

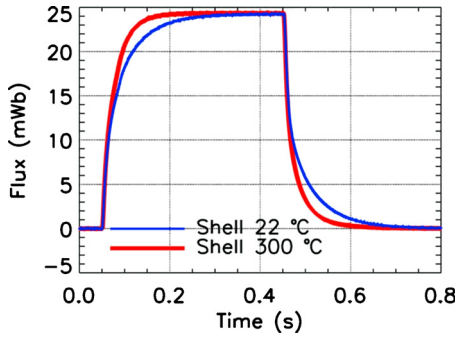


FIG. 5. (Color online) Comparison of signals from a lower, outboard shell flux loop for a long-pulse, square wave, poloidal field-only shot with the shell temperature at 20 °C [dark gray (blue)] and 300 °C [light gray (thick red)].

effect can be noted qualitatively in Fig. 5 by the increase in the rate of the initial rise in the 300 °C calibration shot relative to the rise of the 20 °C calibration shot.

Once the library of calibration shots is populated, calibration signals from the shell flux loops are utilized to diagnose the field null for plasma start-up. The most inboard shell flux loop signal is subtracted from each of the other shell flux loops' signals providing a measure of average field across the annulus defined between the two loops. By focusing on the most outboard and most inboard shell flux loops, the method of shell flux loop subtraction provides a quantification of the field null (or lack thereof) for each shot as a function of time by quantifying the remaining error field across the plasma cross-section. The subtracted signals are analyzed for each calibration shot, and a linear superposition of poloidal fields is designed such that there is a minimal field in each annulus near the peak in loop voltage. This linear superposition can be written as

$$\sum^{i} A_i I(t - t_i) = 0, \tag{2}$$

where the summation is over available poloidal field coil sets, $A$ is the magnitude of the field, and $t_i$ is the coil firing time relative to the Ohmic capacitor bank.

Field contour plots from LTX LRDFIT are compared to the superimposed fields from measured signals to verify the choice of field magnitude, $A_i$, and timing, $t_i$. Discharges are then further designed by simulating current applied to the poloidal field coils and analyzing the resulting field profile plots for regions of good and bad curvature. These latter simulations are necessary for determining pulse-shaping for the long-pulse vertical field coils. The technique of superimposing measured poloidal field-only shots and simulating two-dimensional field contours, coupled with iterative testing of designed fields on the machine, has allowed a suitable field null to be formed, permitting reliable plasma breakdown and start-up (Fig. 6) in the presence of the LTX shell quadrants.

## VI. FUTURE STEPS AND CONCLUSIONS

The two-dimensional representation of LTX in LTX LRDFIT is a valuable tool for initial discharge design. To

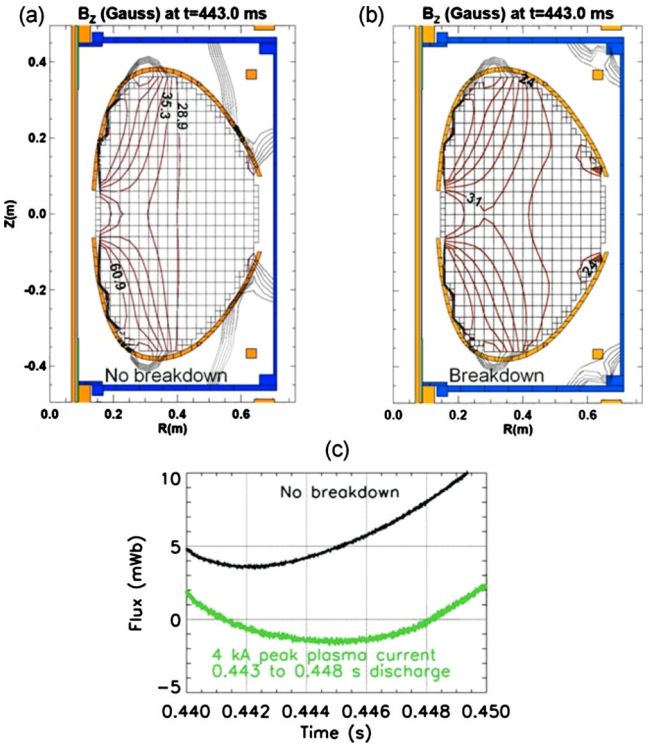


FIG. 6. (Color online) Comparison of simulated vertical field due to experimental poloidal field programming (a) without a suitable null for breakdown and (b) with a suitable null for breakdown (b). (c) The field null, as measured through the shell flux loop subtraction technique, is nonexistent for discharge (a) and present for discharge (b).

model fully the fields and their effects on the plasma, a three-dimensional model and code must now be built. Such a three-dimensional code, CBSHL, is currently under development. CBSHL uses a response function technique[15] coupled with a solution to three-dimensional circuit equations to model vacuum fields and calculate plasma reconstructions.

A three-dimensional triangular mesh of the LTX system has been calculated (Fig. 7), and an exact analytical representation of the field due to a uniform current flowing on a triangular surface has been derived. The linearized circuit

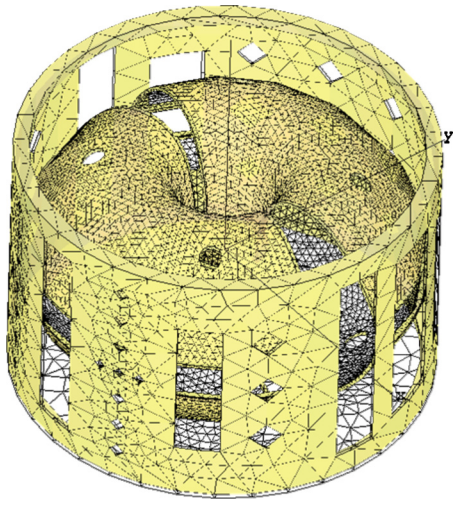

FIG. 7. (Color online) Triangular mesh of shells and vacuum vessel (top flange is removed for clarity) for the three-dimensional code.

equations must now be solved, and the resulting electromagnetic model must be calibrated against LTX vacuum field-only discharges. Once the full code system is completed, three-dimensional, electromagnetic simulations of the double-wall conducting structure of LTX will be possible.

The extensive array of magnetic diagnostics on LTX is now operational. The magnetic diagnostics yield detailed data on magnetic flux and field generated by plasma and eddy currents at multiple toroidal locations and with full poloidal coverage. Reliable breakdown and initial discharge development have been achieved in the presence of a closely coupled, secondary conducting structure utilizing data from the magnetic diagnostics and a two-dimensional approximation for LTX. In addition, the magnetic diagnostics provide data suitable for plasma reconstructions with the two-dimensional code at plasma currents as low as 10 kA with plasma durations on the order of 5 ms.

## ACKNOWLEDGMENTS

This work was supported by the U.S. DOE under Contract No. DE-AC02-09CH11466. L. Berzak was supported by the DOE NNSA Stewardship Science Graduate Fellowship administered by the Krell Institute.

[1] R. W. Moir, Nucl. Fusion **37**, 557 (1997).
[2] N. Morley, S. Smolentsev, R. Munipalli, M. Ni, D. Gao, and M. Abdou, Fusion Eng. Des. **72**, 3 (2004).
[3] S. Mirnov, J. Nucl. Mater. **390–391**, 876 (2009).
[4] D. K. Mansfield, K. W. Hill, J. D. Strachan, M. G. Bell, S. D. Scott, R. Budny, E. S. Marmar, J. A. Snipes, J. L. Terry, S. Batha, R. E. Bell, M. Bitter, C. E. Bush, Z. Chang, D. S. Darrow, D. Ernst, E. Fredrickson, B. Grek, H. W. Herrmann, A. Janos, D. L. Jassby, F. C. Jobes, D. W. Johnson, L. C. Johnson, F. M. Levinton, D. R. Mikkelsen, D. Mueller, D. K. Owens, H. Park, A. T. Ramsey, L. Roquemore, C. H. Skinner, T. Stevenson, B. C. Stratton, E. Synakowski, G. Taylor, A. Von Halle, S. Von Goeler, K. L. Wong, S. J. Zweben, and The TFTR Group, Phys. Plasmas **3**, 1892 (1996).
[5] J. A. Snipes, E. S. Marmar, J. L. Terry, M. G. Bell, R. V. Budny, K. W. Hill, D. Jassby, D. K. Mansfield, D. M. Meade, H. K. Park, J. D. Strachan, B. C. Stratton, E. J. Synakowski, G. Taylor, The TFTR Group, D. N. Ruzic, and M. Shaheen, J. Nucl. Mater. **196–198**, 686 (1992).
[6] D. Strachan, K. Mansfield, G. Bell, J. Collins, D. Ernst, K. Hill, J. Hosea, J. Timberlake, M. Ulrickson, J. Terry, E. Marmar, and J. Snipes, J. Nucl. Mater. **217**, 145 (1994).
[7] S. Mirnov, Fusion Eng. Des. **65**, 455 (2003).
[8] M. L. Apicella, G. Mazzitelli, V. Pericoli Ridolfini, V. Lazarev, A. Alekseyev, A. Vertkov, R. Zagorski, and FTU Team, J. Nucl. Mater. **363–365**, 1346 (2007).
[9] R. Majeski, R. Kaita, M. Boaz, P. Efthimion, T. Gray, B. Jones, D. Hoffman, H. Kugel, J. Menard, and T. Munsat, Fusion Eng. Des. **72**, 121 (2004).
[10] R. Majeski, R. Doerner, T. Gray, R. Kaita, R. Maingi, D. Mansfield, J. Spaleta, V. Soukhanovskii, J. Timberlake, and L. Zakharov, Phys. Rev. Lett. **97**, 075002 (2006).
[11] L. Berzak, R. Kaita, T. Kozub, R. Majeski, and L. Zakharov, Rev. Sci. Instrum. **79**, 10F116 (2008).
[12] J. Menard, R. Bell, D. Gates, S. Kaye, B. LeBlanc, F. Levinton, S. Medley, S. Sabbagh, D. Stutman, K. Tritz, and H. Yuh, Phys. Rev. Lett. **97**, 095002 (2006).
[13] H. Y. Yuh, F. M. Levinton, R. E. Bell, J. C. Hosea, S. M. Kaye, B. P. LeBlanc, E. Mazzucato, J. L. Peterson, D. R. Smith, J. Cy, R. E. Waltz, C. W. Domier, N. C. Luhmann, W. Lee, and H. K. Park, Phys. Plasmas **16**, 056120 (2009).
[14] A. A. Istratov and O. F. Vyvenko, Rev. Sci. Instrum. **70**, 1233 (1999).
[15] J. Spaleta, L. Zakharov, R. Kaita, R. Majeski, and T. Gray, Rev. Sci. Instrum. **77**, 10E305 (2006).

The Princeton Plasma Physics Laboratory is operated
by Princeton University under contract
with the U.S. Department of Energy.

Information Services
Princeton Plasma Physics Laboratory
P.O. Box 451
Princeton, NJ 08543

Phone: 609-243-2245
Fax: 609-243-2751
e-mail: pppl_info@pppl.gov
Internet Address: http://www.pppl.gov